

SHI, H., WANG, S., FERNANDEZ, C., YU, C., FAN, Y. and CAO, W. 2021. Improved splice-electrochemical circuit polarization modeling and optimized dynamic functional multi-innovation least square parameter identification for lithium-ion batteries. *International journal of energy research [online]*, 45(10), pages 15323-15337. Available from: <https://doi.org/10.1002/er.6807>

Improved splice-electrochemical circuit polarization modeling and optimized dynamic functional multi-innovation least square parameter identification for lithium-ion batteries.

SHI, H., WANG, S., FERNANDEZ, C., YU, C., FAN, Y. and CAO, W.

2021

This is the peer reviewed version of the following article: SHI, H., WANG, S., FERNANDEZ, C., YU, C., FAN, Y. and CAO, W. 2021. Improved splice-electrochemical circuit polarization modeling and optimized dynamic functional multi-innovation least square parameter identification for lithium-ion batteries. International journal of energy research [online], 45(10), pages 15323-15337, which has been published in final form at <https://doi.org/10.1002/er.6807>. This article may be used for non-commercial purposes in accordance with [Wiley Terms and Conditions for Use of Self-Archived Versions](#)

Improved splice-electrochemical circuit polarization modeling and optimized dynamic functional multi-innovation least square parameter identification for lithium-ion batteries

Haotian Shi, Shunli Wang, Carlos Fernandez, Chunmei Yu, Yongcun Fan, Wen Cao

School of Information Engineering, Southwest University of Science and Technology, Mianyang, China,

School of Pharmacy and Life Sciences, Robert Gordon University, Aberdeen, UK

Correspondence: Shunli Wang, School of Information Engineering, Southwest University of Science and Technology, Mianyang 621010, China. Email: wangshunli@swust.edu.cn

Funding information National Natural Science Foundation of China, Grant/Award Number: 61801407

Summary

The internal nonlinearity of the lithium-ion battery makes its mathematical modeling a big challenge. In this paper, a novel lithium-ion battery splice electrochemical circuit polarization (S-ECP) model is proposed, which integrates the strengths of various lithium-ion battery models and refines the ohm and polarization characteristics of the electrochemical Nernst model and the differences in charge-discharge internal resistance. Moreover, by applying the one-sided limit to the discrete system, a multi-innovation least squares algorithm optimized based on the dynamic function (F-MILS) introduced to constrain the original innovation weight is put forward, which tackles the problem of large algorithm errors caused by huge changes in the system input. In order to evaluate the regulating ability of weight constraint factors, the relevant parameter values in the dynamic function are discussed as independent variables. Furthermore, parameters of the S-ECP model are identified online by HPPC experimental data combined with the multi-innovation least squares(MILS) algorithm ameliorated by the dynamic function, and the convergence speed of parameters in the identification process is analyzed. Finally, an urban dynamometer driving schedule experiment is carried out on the lithium-ion battery under more complex working conditions. It is revealed that the accuracy of F-MILS is 0.5% higher than that of unoptimized MILS, further confirming the accuracy of the S-ECP model and the superiority of the F-MILS algorithm.

KEYWORDS: dynamic function optimization, lithium-ion batteries, multi-innovation least squares, parameter identification, splice-electrochemical circuit polarization model

1 | INTRODUCTION

1.1 | Motivation and challenges

With the rapid development of electric vehicles in recent years, battery energy storage technology has gained increasing concern and demonstrated its great values in practice.¹ Lithium-ion batteries are widely applied power batteries at present due to the advantages of high energy density, long cycle life, high output voltage, and high-rate charge-discharge ability.² The state of charge (SOC) estimation of the battery is the basis of the battery management system (BMS), and the estimation accuracy is an important index to measure the quality of the BMS. The establishment of a high-fidelity battery model and the result of high-precision parameter identification are the prerequisites for obtaining an accurate SOC. Therefore, the construction of an accurate battery model and precise parameter identification are the key to the BMS.

1.2 | Literature review

Electrochemical models and equivalent circuit models are extensively used among diverse lithium-ion battery models, but both merits and drawbacks of these two models are extreme. For improving the accuracy of lithium-ion battery models, a nonlinear model is proposed to accurately describe the external properties of lithium-ion batteries; it lays the foundation for the accuracy of nonlinear battery SOC estimation, but the calculation of this method is relatively complicated.⁴ The asymptotic reduction and homogenization principles of lithium-ion battery electrochemical models are discussed to increase anti-interference ability of the models.⁵ Through the modeling of aviation lithium-ion battery pack, a safety prediction method based on real-time detection and filtering is proposed, which greatly improves the safety factor of lithium-ion battery use in the aviation field.⁶ The fractional order model of lithium-ion batteries was investigated and compared with the integer order model in terms of prediction accuracy, which improves the SOC estimation accuracy of the nonlinear battery.^{7,8} The simplified fractional equivalent circuit model of lithium-ion battery is analyzed, and the model parameters are identified online by adaptive technology, which enhances the adaptability of the BMS system.⁹ An unbiased model of battery noise immunity is established, which reduces the common noise problem of parameterized models.¹⁰ A mixture model taking current, voltage, and temperature as input of lithium-ion batteries was provided, which had prospective applications in battery SOC estimation under complex working conditions.¹¹ Through Thevenin modeling of liquid metal battery, the online parameter identification method under this model is studied, which laid a theoretical basis for the development of the application potential of electric energy storage systems.¹² The model of the lithium iron phosphate battery for pure electric vehicles and the strategies for identifying the model parameters are offered, which greatly improves the use efficiency of vehicle batteries.¹³ Using the correlation between the states, cooperative estimation strategy and the prediction of the state of charge based on unscented particle filtering are proposed, which greatly improves the estimation accuracy of the battery state.^{14,15} The charge of

the comprehensive model constructed in three different states of lithium-ion battery was estimated and compared, and a summary review of the state estimation methods commonly used in BMS was made.^{16,17} Although the lithium-ion battery model and adaptive iterative calculation method are given, the efficiency of the battery is increased to a certain extent.^{18,19} But with the deepening of the application of lithium-ion batteries, higher requirements are put forward for the accuracy and stability of the model, which requires the design of a new model to improve the performance of the lithium-ion battery. A lithium-ion battery dynamic model that could well simulate the dynamic interaction between battery aging and electric heating is provided for electric vehicles.²⁰ The operando 3-omega sensor is employed to identify and characterize the internal thermal resistance of lithium-ion batteries, capable of improving the accuracy of the battery model.²¹ The electrochemical impedance and nuclear magnetic resonance spectra are analyzed to determine the stability of the electrolyte in lithium-air batteries, which provided reference for accurate modeling of lithium-ion batteries.²² A load response model for lithium-ion batteries at the charging state was proposed and applied to SOC estimation,²³ and lithium-ion hybrid capacitors at different temperatures were modeled, which offered guidance for the design of the device for estimating succeeding states.^{24,25} By modeling the series lithium-ion battery pack and considering the change of temperature, a model-based battery SOC estimation method was proposed, which realizes the accurate estimation of the SOC of lithium-ion batteries under complex temperature conditions.²⁶ In addition, through the establishment of a lithium-ion battery nonlinear model and a fractional order model, and applying them to the SOC estimation of electric vehicles, the accurate state of the effective state of electric vehicles is improved.^{27,28} Taking into account the degree of polarization of the lithium-ion battery, accurate identification of the parameters of the battery's charging state and the state of health under complex operating conditions is realized.²⁹ By establishing a nonlinear degradation model, the energy storage effect and efficiency of lithium-ion batteries have been greatly improved.³⁰ In addition to the above-mentioned lithium-ion battery model, researchers have established numerous intelligent models for the internal nonlinear characteristics of the battery and considering the coupling of internal and external factors. And the above model is used to estimate the state of battery health or state of charge. It improves the modeling accuracy and ensures the high fidelity between the battery and the model, providing a theoretical basis for the subsequent prediction of the battery state.³¹⁻³⁸

1.3 | Contributions

Compared with the above equivalent circuit models, electrochemical models based on the electrochemical reaction mechanism are described by mathematical relationships inside the battery. They are capable of essentially reflecting external battery parameters and the internal relationship between the electrochemical reactions, fully characterizing the battery, elevating the model prediction accuracy, and estimating the battery state more precisely. However, the traditional pure electrochemical model is difficult to simulate the dynamic performance of the battery. In this article, taking both accuracy and computational complexity of characterization into account, the lithium-ion battery splice-electrochemical circuit polarization model that combines electrochemical and equivalent circuits and possesses the merits of different equivalent circuit models is built, which has higher accuracy of describing the working status of the lithium-

ion battery. To solve the time-consuming problem and large errors of traditional parameter identification approaches as well as the data saturation problem possibly existing in the multi-innovation least squares algorithm, with the one-sided limit applied in the discrete system, a multi-innovation least squares algorithm optimized by the dynamic function introduced to constrain the original innovation weight is proposed. F-MILS improves the data utilization efficiency and accelerates the algorithm convergence. The parameters of the S-ECP model are identified by using hybrid pulse power characterization (HPPC) data with the help of the F-MILS. The accuracy of F-MILS is verified by the urban dynamometer driving schedule (UDDS) condition experiment, which provides data and a theoretical basis for future S-ECP and FMILS-based SOC estimation of lithium-ion batteries.

2 | THEORETICAL ANALYSIS

2.1 | The equivalent model

Typical electrochemical models mainly include Shepherd model, Unnewehr model, Nernst model, etc. The empirical equation of the model is constructed by analyzing the physical mechanism and electrochemical reactions inside the battery. In order to simplify the computation of the battery equivalent model and improve the simulation accuracy, the simplified empirical model is widely used. By the exploratory application of empirical equations and parameter identification, equivalent characterization of the battery state is achieved. Mathematical expressions of typical electrochemical models are presented in Table 1. Due to the transition process and polarization reaction in the charging and discharging process of lithium-ion batteries, the battery has excellent dynamic performance. The resistance-capacitance (RC) equivalent circuit model can simulate the dynamic performance of the battery through the RC parallel network, which has strong versatility and scalability. However, the increased RC networks will result in large quantities of computation and the over-fitting problem (Table 2). In order to balance the calculation and the accuracy of parameter identification, we construct a novel S-ECP model based on the first-order RC equivalent circuit model in this paper after refining the ohm and polarization characteristics of Nernst model and the differences in charge discharge internal resistance of lithium-ion batteries. The S-ECP model structure is shown in Figure 1.

In Figure 1, R_0 is ohm resistance, R_p is polarization resistance, C_p is polarization capacitance, R_c is internal resistance at charging, R_{cd} is the internal resistance of the battery during charging and discharging, in which the internal resistance during discharging is represented by R_d , and the internal resistance during charging is represented by R_c . I is charge and discharge current, and the discharge direction is set as the positive direction. U is the sum of voltage at both ends of the R_0 and RC parallel circuit. The electrodynamic force of the S-ECP model comes from Nernst empirical equation, of which the functional value is used to represent the open circuit voltage U_{oc} of the battery. U_L is the port voltage of the lithium-ion battery. The equivalent mechanism of each part of the S-ECP model proposed is described as follows:

2.2 | Open-circuit voltage equivalent analysis

For better accuracy of parameter identification, we optimize the ohm and polarization characteristics of Nernst model. In combination with the equivalent circuit model, an S-ECP model with the improved Nernst model as the open-circuit voltage is proposed. Experiments show that Nernst model performs better in fitting in the whole charging and discharging process.

In view of the special working condition of lithium-ion batteries, different combination tests suggest that K_0 , K_1 , and K_2 constants selected by the model can well fit the data. An S-ECP model-based open-circuit voltage function curve is plotted by multivariate function fitting of relevant laboratory data.

2.3 | State space description analysis

Based on S-ECP in Figure 1 and Kirchhoff's circuit law, the relationship of electrical quantities at t is given, as shown in Equation (1).

$$\begin{cases} U_L(t) = U_{OC} - U_P(t) - I(t)R_0 - I(t)R_{cd} \\ dU_P(t)/dt = I(t)/C_P - U_P(t)/(C_P R_P) \\ U_{OC} = K_0 + K_1 \ln(\text{SOC}) + K_2 \ln(1 - \text{SOC}) \end{cases} \quad (1)$$

where $U_L(t)$ is terminal voltage of the battery at t , and t is the continuous time constant.

The state space equation of the system obtained from the S-ECP model is a continuous time model, which is not applicable to online parameter identification, so we discretize Equation (1) according to the procedures shown in Figure 2.

In combination with Figure 2, we have the difference equation of the discretized system as Equation (2).

$$U(k) = \frac{R_p C_p}{R_p C_p + T} U(k-1) + \left(R_0 + \frac{R_p}{R_p C_p + T} \right) I(k) - \frac{R_0 R_p C_p}{R_p C_p + T} I(k-1) \quad (2)$$

where T is the sampling period and k is the discrete time constant. The matrices of coefficients and parameter to be identified can be obtained by the difference equation. Equation (3) expresses the matrices

$$\begin{cases} \theta = [a_1, a_2, a_3] = \left[-\frac{R_p C_p}{R_p C_p + T}, R_0 + \frac{R_p}{R_p C_p + T}, -\frac{R_0 R_p C_p}{R_p C_p + T} \right] \\ \eta = [R_0, R_p, C_p, R_{cd}] = \left[\frac{b_1}{a_1}, \frac{a_1 b_1 - b_2}{a_1(a_1 + 1)}, -\frac{a_1^2 T}{a_1 b_1 - b_2}, R_{nom} - \frac{b_1}{a_1} \right] \end{cases} \quad (3)$$

where θ and η are the matrices of coefficients and parameter to be identified of the discrete system model, respectively. R_{nom} is a direct measurement of the normal mixed resistance value after being completely put aside. By making the difference between the measured value of R_{nom} and the identification value of R_0 under different SOC values, the R_{cd} value of the battery under different SOC values can be easily identified.

Then, the autoregressive exogenous (ARX) model for online parameter identification of lithium-ion batteries is achieved, as shown in Equation (4).

$$y(k) = \beta^T(k) \theta \Leftarrow \begin{cases} \theta = [a_1, a_2, a_3] \\ \beta(k) = [U(k-1), I(k), I(k-1)] \end{cases} \quad (4)$$

where β , $y(k)$, and $I(k)$ are the data vector, output, and input of the discrete system model, respectively. The coefficient matrix θ of the discrete system model is identified by MILS. According to Equation (4), all the parameters to be identified in the S-ECP model are acquired by recursion.

2.4 | Parameter identification method analysis

To solve the problem of data saturation in parameter identification of the recursive least squares algorithm and large errors of MILS caused by huge system input variations, we propose an F-MILS based on the dynamic function introduced to modify the matrix innovation of MILS. F-MILS can dynamically adjust the system with the preset function when the input differs greatly, capable of improving the data utilization efficiency and accelerating algorithm convergence.

2.4.1 | MILS algorithm model derivation

MILS identification algorithm extends the scalar innovation to vector innovation and a data vector to an information matrix on the basis of the traditional RLS identification algorithm. It identifies system parameters by online iteration. The model that is applicable to this algorithm is derived in Figure 3.

According to Figure 3, if we assume the ARX model as Equation (5):

$$A(z^{-1})y(k) = B(z^{-1})u(k) + e(k) \quad (5)$$

where $y(k)$ is the output sequence of the system, $u(k)$ is the input sequence of the system, $e(k)$ is the Gaussian white noise with zero mean, $A(z^{-1})$ and $B(z^{-1})$ are delay operator polynomials of order n_a and order n_b , respectively, and they are expressed as:

$$\begin{cases} A(z^{-1}) = 1 + a_1z^{-1} + a_2z^{-2} + \dots + a_{n_a}z^{-n_a} \\ B(z^{-1}) = b_0 + b_1z^{-1} + b_2z^{-2} + \dots + b_{n_b}z^{-n_b} \end{cases} \quad (6)$$

The discrete transfer function of the system is:

$$G(z^{-1}) = \frac{B(z^{-1})}{A(z^{-1})} = \frac{b_0 + b_1z^{-1} + b_2z^{-2} + \dots + b_{n_b}z^{-n_b}}{1 + a_1z^{-1} + a_2z^{-2} + \dots + a_{n_a}z^{-n_a}} \quad (7)$$

Then, we transform the discrete transfer function into a difference equation:

$$y(k) = -\sum_{i=1}^{n_a} a_i y(k-i) + \sum_{i=1}^{n_b} b_i u(k-i) + e(k) \quad (8)$$

Taking θ as the coefficient matrix of the model, the expression is shown in Equation (9).

$$\boldsymbol{\theta} = [-a_1, -a_2, \dots, -a_{n_a}, b_0, b_1, \dots, b_{n_b}] \quad (9)$$

Then, the scalar innovation of the system is described as Equation (10).

$$v(k) = y(k) - \boldsymbol{\beta}^T(k) \hat{\boldsymbol{\theta}}(k-1) \quad (10)$$

where $\boldsymbol{\beta}^T(k)$ is the data vector of the current moment, and $\hat{\boldsymbol{\theta}}(k-1)$ is the estimated value of the coefficient matrix at the previous moment.

After expanding the scalar innovation, the resulting matrix innovation is expressed by Equation (11).

$$\mathbf{V}(n_p, k) = \begin{bmatrix} y(k) - \boldsymbol{\beta}^T(k) \hat{\boldsymbol{\theta}}(k-1) \\ y(k-1) - \boldsymbol{\beta}^T(k-1) \hat{\boldsymbol{\theta}}(k-2) \\ \vdots \\ y(k-n_p+1) - \boldsymbol{\beta}^T(k-n_p+1) \hat{\boldsymbol{\theta}}(k-n_p) \end{bmatrix} \quad (11)$$

where n_p is the length of innovation.

Then, we obtain the model applicable to MILS, as represented in Equation (12).

$$\mathbf{Y}(n_p, k) = \boldsymbol{\beta}^T(n_p, k) \boldsymbol{\theta}(k-1) + \mathbf{V}(n_p, k) \quad (12)$$

where $\mathbf{Y}(n_p, k)$ is the system output vector after innovation modification.

2.4.2 | Dynamic function improvement

The simulation results under complex dynamic conditions show that the parameter identification of the SECP model by MILS has big errors when the input current change rate is large. Besides, a sudden change of the system state will lead to an unsatisfactory tracking effect of terminal voltage of the model during the online parameter identification of MILS, thereby further reducing the accuracy of parameter identification and the subsequent SOC estimation precision. To tackle the above-mentioned problems, we propose an F-MILS based on the dynamic function introduced to constrain the original and innovation weight by optimizing the innovation of MILS. F-MILS tremendously improves the tracking effect of terminal voltage at a large input current change rate. The specific improvement principle of F-MILS is shown below.

The one-sided limit of the input current of the system is defined as Equation (13):

$$\begin{aligned} f_{I-}'(t) &= \lim_{\Delta t \rightarrow T^-} \frac{\Delta I}{\Delta t} = \lim_{\Delta t \rightarrow T^-} \frac{f_I(k+\Delta t) - f_I(k)}{\Delta t} \\ &= \lim_{\Delta t \rightarrow T^-} \frac{I(k) - I(k-1)}{\Delta t} \end{aligned} \quad (13)$$

where $f_{I-}(t)$ is the one-sided change rate of current in two consecutive steps.

If the system current change rate is high and meets the following constraints:

$$f'_{I-}(t) \geq f'_{I-}(t)_{\max} \quad (14)$$

The optimized innovation matrix is:

$$\begin{cases} \mathbf{V}_{\text{imp}}(n_p, k) = g(I)\mathbf{V}(n_p, k) \\ g(I) = \left(\gamma + \alpha^{\frac{1}{|I_k - I_{k-1}|}} \right) \end{cases} \quad (15)$$

where γ is the constant factor in the dynamic function, α is the base factor in the dynamic function, which takes the value of $\alpha \in (0, 1)$, $g(I)$ is the weight constraint factor, which takes the value of $g(I) \in (1, 2)$ to prevent the occurrence of soft regulation and over regulation, and $1/(|I_k - I_{k-1}|)$ is the reciprocal of the current change rate, which takes the value of $1/(|I_k - I_{k-1}|) \in (0, 1)$ in the case of abrupt change of current.

Then, the model applicable to F-MILS is represented as Equation (16).

$$\mathbf{Y}_{\text{imp}}(n_p, k) = \boldsymbol{\beta}^T(n_p, k)\boldsymbol{\theta}(k-1) + \mathbf{V}_{\text{imp}}(n_p, k) \quad (16)$$

where $\mathbf{V}_{\text{imp}}(n_p, k)$ is the improved innovation matrix.

2.4.3 | Parameter identification based on F-MILS

To enhance the tracking effect of terminal voltage at a large input current change rate, we apply the one-sided limit to the discrete system and design an F-MILS based on the dynamic function introduced to constrain the original and innovation weight. F-MILS enables the innovation to adaptively match the system input change rate and further generates different weight constraints on the innovation, thus notably elevating the innovation utilization efficiency, speeding up the algorithm convergence and increasing the parameter identification accuracy. According to the last section, we can derive the recursive process of F-MILS, as shown in Figure 5.

According to Figure 4, the recursive process of parameter identification based on F-MILS is described in Table 3.

3 | EXPERIMENT ANALYSIS

3.1 | Experimental platform and battery parameters

This study takes a ternary polymer lithium-ion battery with a nominal capacity of 50 Ah as the subject. To verify the accuracy of the S-ECP model and the superiority of F-MILS, we use the existing equipment in the laboratory to build a small-scale test platform. Figure 5 delineates the structure of the experimental device.

As shown in Figure 5, the structure of the experimental device includes: (a) temperature cycle test chamber (BTKS5-150C), whose temperature range is 40~ 150°C; (b) power battery module test system (BTS750-200-100-4); (c) simulated high-altitude low-voltage test chamber (BE8104); and (d) BMS performance test system (CCS-5V600A and BMS-HIL-1005).

3.2 | Feasible region of weight constraint factors

To deal with the parameter identification error caused by a large input current change rate of the discrete system, an F-MILS based on the dynamic function introduced to constrain the original and innovation weight is proposed, which improves the tracking effect of terminal voltage in the condition that the input current change rate is large. In order to evaluate the regulating ability of weight constraint factors, the parameter values in the dynamic function are discussed with α and $1/|I_k - I_{k-1}|$ as independent variables. In this way, the best regulating effect of weight constraint factors is achieved while avoiding the over regulation. The discussion results are shown in Figure 6.

In Figure 6, x represents $1/|I_k - I_{k-1}|$, y stands for α , and z denotes $g(I)$. As indicated in the figure, weight constraint factors are all less than 1 when $\gamma < 1$, resulting in soft regulation. Under a large system input current change rate, weight constraint factors less than 1 leads to big system errors, rather than regulates the system. Therefore, soft regulation should be prevented. When $\gamma > 1$, weight constraint factors are all greater than 1, causing over regulation and enlarging the system error. When $\gamma = 1$, the overall range of weight constraint factors is $g(I)$ (1.0, 2.0) (Figure 7C), which can help prevent soft regulation and over regulation. The reason is that in this range, the weight constraint factors change adaptively with the system current input and thus are suitable for the research on online parameter identification of lithium-ion batteries. Therefore, $\gamma = 1$ is selected for the following F-MLIS-based online parameter identification studies.

3.3 | Parameter identification results

We conduct an intermittent charge-discharge experiment on the battery to examine the accuracy of the S-ECP model and the superiority of F-MILS, with a capacity of 5% at each time. After the battery is put aside for 2 h, the battery resistance is measured by a high-precision battery internal resistance tester. The average R_{nom} when charging the battery is 3.9443 m ω , and the average R_{nom} when discharging is 5.4631 m ω . Since the R_0 of the battery is relatively stable during charging and discharging, this study assumes that the R_0 of the battery during charging is the same as the R_0 during discharging. On this basis, according to the parameter identification results of FMILS, the R_c and R_d of the S-ECP model can be calculated. Additionally, the terminal voltage of the battery after standing is detected using a voltage tester during each intermittent charge-discharge experiment. Based on experimental data, the parameters of the improved Nernst model are identified. Table 4 describes the identification results and errors.

The S-ECP model-based OCV-SOC curve is plotted based on the identification results in Table 4. The data obtained by the standard HPPC experiment identify parameters and validate the S-ECP model. The HPPC experiment steps are given in Table 5.

The charge-discharge tests of the lithium-ion battery are conducted following the above test steps to afford the current, terminal voltage, and SOC waveforms in the HPPC test. Then, the parameters of the S-ECP model are identified online by F-MILS. The results are shown in Figure 7.

In Figure 7A-D show the current curve, the voltage curve, and the SOC curve of the HPPC test, respectively. Figure 7E,G,I illustrate the parameter identification results of the S-ECP model. Figure 7F,H,J are the convergence rates of parameters during F-MILS-based identification. Figure 7K,L are the terminal voltage comparison curve and the terminal voltage error comparison curve of the HPPC test, respectively. In the two figures, U_1 , U_2 , and U_3 denote the actual terminal voltage, the terminal voltage obtained by MILS, and the terminal voltage obtained by F-MILS, respectively. It can be seen from Figure 7E,G,I that at the initial stage of discharging, R_0 is small (about $1.4 \text{ m}\Omega$), R_p is larger (about $0.5 \text{ m}\Omega$), and C_p is small (about 600F). In the middle and later stages of discharging, R_0 and C_p increase while R_p decreases. At the end of discharging, C_p declines slightly. According to Figures 7F,H,J, F-MILS has a slow convergence speed and the curve fluctuates greatly at the initial stage of discharging. However, as the experiment continues, the convergence of each parameter is accelerated, the curve fluctuates slightly, and the parameter identification gets more precise. As shown in Figure 7K,L, the maximum errors of MILS and F-MILS are 4.7% and 1.6%, respectively, in the whole HPPC test. That is to say, the accuracy of F-MILS is 3.1% higher than that of the unmodified MILS. Moreover, the terminal voltage obtained by F-MILS can better track the actual terminal voltage. The HPPC experiment not only confirms the feasibility of S-ECP model but also preliminarily demonstrated the superiority of F-MILS.

3.4 | F-MILS algorithm verification

To further prove the superiority of F-MILS and the correction effectiveness of weight adjustment factors at a large current change rate, we carry out UDDS experiment on the lithium-ion battery under more complex working conditions and compare the terminal voltage tracking error measured by MILS with the MILS results. The current, voltage, and SOC curves of the UDDS experiment are shown in Figure 8. In Figure 8A-D the current curve, the voltage curve, and the SOC curve of the UDDS test, respectively. Figure 8E,F show the terminal voltage comparison curve and the terminal voltage error comparison curve of the HPPC test, respectively. In these two figures, U_1 , U_2 , and U_3 represent the actual terminal voltage, the terminal voltage obtained by MILS, and the terminal voltage obtained by F-MILS, respectively. It can be seen from Figure 8A that the current changes more frequently under UDDS conditions although the change rate under such conditions is not as high as that of the HPPC experiment. Meanwhile, the current change rates at adjacent moments vary, indicating that the UDDS test is more applicable to the verification of the regulating ability of weight constraint factors. According to Figure 8E,F, F-MILS has a big error at the initial stage of the experiment, and the maximum error is 0.2%, which is 0.5% smaller than that of MILS (0.7%). As the experiment keeps going on, the terminal voltage errors of MILS and F-MILS decrease to 0.35% and 0.14%, respectively. F-MILS is still more accurate than MILS. In addition, the maximum error of parameter identification by S-ECP model combined with F-MILS algorithm is 11 mV, 0.3% higher than that by Reference 39 (the maximum error is 25 mV) and 0.2% higher than that by Reference 40 (the maximum error is 20 mV). Taken together, under the working environment of high current density and current rate of change, the S-ECP model and F-MILS algorithm proposed in this paper are better than the traditional ECMs and MILS algorithms.

4 | CONCLUSION

This paper aims to precisely describe the working status of lithium-ion batteries and improve the identification efficiency of lithium-ion parameters. Combining the advantages of different lithium-ion battery models and considering the model's characterization accuracy and the computational complexity of parameter identification, an S-ECP model that can more accurately describe the working status of lithium-ion batteries is proposed. To tackle the possible data saturation problem of MILS and the slow convergence problem caused by huge changes in the system input, we apply one-sided limit to the discrete system and put forward an F-MILS based on the dynamic function introduced to constrain the original and innovation weight and considers the influence of noise on identification accuracy. F-MILS can dynamically adjust the system with the preset function when a huge input change occurs, capable of improving the data utilization efficiency and accelerating the algorithm convergence. HPPC and UDDS experiments show that the maximum errors of the F-MILS and MILS algorithms at the initial stage of battery discharge are 0.2% and 0.7, respectively, and the maximum errors of the FMILS and MILS algorithms at the later stage of the battery discharge are 0.35% and 0.14%, respectively. The accuracy of the S-EP model and the superiority of the FMILS algorithm are verified. Future work will focus on SOC estimation based on the S-ECP model and F-MILS.

ACKNOWLEDGMENTS

This research was supported by National Natural Science Foundation (No. 61801407). Thanks to the sponsors. CF would like to express his gratitude to RGU for its support.

CONFLICT OF INTEREST

The authors declare that they have no known competing financial interests or personal relationships that could have appeared to influence the work reported in this paper.

ORCID: Shunli Wang <https://orcid.org/0000-0003-0485-8082>

REFERENCES

1. Wang Y, Sun Z, Chen Z. Development of energy management system based on a rule-based power distribution strategy for hybrid power sources. *Energy*. 2019;175:1055-1066.
2. Liu W, Niu S, Xu H. Optimal planning of battery energy storage considering reliability benefit and operation strategy in active distribution system. *J Mod Power Syst Clean Energy*. 2017;5(2):177-186.
3. Yang F, Song X, Dong G, Tsui KL. A coulombic efficiency based model for prognostics and health estimation of lithium ion batteries. *Energy*. 2019;171:1173-1182.
4. Meng JH, Stroe DI, Ricco M, Luo GZ, Teodorescu R. A simplified mode based state-of-charge estimation approach for lithium-ion battery with dynamic linear model. *IEEE Trans Ind Electron*. 2019;66(10):7717-7727.
5. MGH A, IRM B. Asymptotic reduction and homogenization of a thermo-electrochemical model for a lithium-ion battery. *AppMath Model*. 2020;80:724-754.
6. Wang SL, Carlos F, Chen MJ, Wang L, Su J. A novel safety anticipation estimation method for the aerial lithium-ion battery pack based on the real-time detection and filtering. *J Clean Prod*. 2018;185:187-197.
7. Tian J, R Xiong, Q Yu. Fractional-order model-based incremental capacity analysis for degradation state recognition of lithium-ion batteries. *IEEE Trans Ind Electron*. 2019;66(2):1576-1584.
8. Zou Y, Li SBE, Shao B, Wang BJ. State-space model with noninteger order derivatives for lithium-ion battery. *Appl Energy*. 2016; 161:330-336.
9. Wang JL, Zhang L, Xu D, Zhang P, Zhang GR. A simplified fractional order equivalent circuit model and adaptive online parameter identification method for lithium-ion batteries. *Math Probl Eng*. 2019;2019(10):1-8.
10. Wei ZB, Zhao D, He H, Cao W, Dong G. A noise-tolerant model parameterization method for lithium-ion battery management system. *Appl Energy*. 2020;268:114932.
11. Liu DT, Li L, Song YC, Wu LF, Peng Y. Hybrid state of charge estimation for lithium-ion battery under dynamic operating conditions. *Int J Electr Power Energy Syst*. 2019;110:48-61.
12. Liu GA, Xu C, Li HM, Jiang K, Wang KL. State of charge and online model parameters co-estimation for liquid metal batteries. *Appl Energy*. 2019;250:677-684.
13. Wang S, Chen QZ, Wang K, Wang ZY, Wang Y. Parameter identification of lithium iron phosphate battery model for battery electric vehicle. *IOP Conf Mater Sci Eng*. 2019;677:032048.

14. Shen P, Ouyang MG, Lu LG, Li JQ, Feng XN. The co-estimation of state of charge, state of health and state of function for lithium-ion batteries in electric vehicles. *IEEE Trans Veh Technol.* 2017;67:92-103.
15. Wang YJ, Chen ZH. A framework for state-of-charge and remaining discharge time prediction using unscented particle filter. *Appl Energy.* 2020;260:114324.
16. Wei ZB, Zhao JY, Zou CF, Lim TM, Tseng KJ. Comparative study of methods for integrated model identification and state of charge estimation of lithium-ion battery. *J Power Sources.* 2018;402:189-197.
17. Wang YJ, Tian JQ, Sun ZD, et al. A comprehensive review of battery modeling and state estimation approaches for advanced battery management systems. *Renew Sustain Energy Rev.* 2020; 131:110015.
18. Wang SL, Fernandez C, Cao W, Zou CY, Yu CM, Li XX. An adaptive working state iterative calculation method of the power battery by using the improved Kalman filtering algorithm and considering the relaxation effect. *J Power Sources.* 2019;428:67-75.
19. Wang YJ, Liu C, Pan R, Chen ZH. Modeling and state-of-charge prediction of lithium-ion battery and ultracapacitor hybrids with a co-estimator. *Energy.* 2017;121:739-750.
20. Mesbahi T, Rizoug N, Bartholomeus P, Sadoun R, Khenfri F, Le Moigne P. Dynamic model of Lithium-ion batteries incorporating electrothermal and ageing aspects for electric vehicle applications. *IEEE Trans Ind Electron.* 2017;65(2):1298-1305.
21. Lubner SD, Kaur S, Fu YB, Battaglia V, Prasher RS. Identification and characterization of the dominant thermal resistance in lithium-ion batteries using operando 3-omega sensors. *J Appl Phys.* 2020;127(10):105104.
22. Dornbusch DA, Viggiano RP, Lvovich VF. Integrated impedance-NMR identification of electrolyte stability in lithium-air batteries. *Electrochim Acta.* 2020;349:136169.
23. Tang XP, Gao FR, Zou CF, Yao K, Hu WG, Wik T. Load-responsive model switching estimation for state of charge of lithium-ion batteries. *Appl Energy.* 2019;238:423-434.
24. Li XY, Huang ZJ, Tian Y, Tian JD. Modeling and comparative analysis of a lithium-ion hybrid capacitor under different temperature conditions. *Int J Energy Res.* 2020;44(5):3801-3820.
25. Yang H, Sun XZ, An YB, Zhang X, Wei TZ, Ma YW. Online parameters identification and state of charge estimation for lithium-ion capacitor based on improved cubature Kalman filter. *J Energy Storage.* 2019;24:100810.
26. Huang DY, Chen Z, Zheng CW, Li HB. A model-based state-of-charge estimation method for series-connected lithium-ion battery pack considering fast-varying cell temperature. *Energy.* 2019;185:847-861.
27. Kim WY, Lee PY, Kim J, Kim KS. A nonlinear-model-based observer for a state-of-charge estimation of a lithium-ion battery in electric vehicles. *Energies.* 2019;12(17):3383.

28. Xiong R, Tian J, Shen W, Sun F. A novel fractional order model for state of charge estimation in lithium-ion batteries. *IEEE Trans Veh Technol.* 2019;68(5):4130-4139.
29. Xia B, Chen G, Zhou J, Yang Y, Wang H. Online parameter identification and joint estimation of the state of charge and the state of health of lithium-ion batteries considering the degree of polarization. *Energies.* 2019;12(15):2939.
30. Maheshwari A, Paterakis NG, Santarelli M, Gibescu M. Opti-mizing the operation of energy storage using a non-linear lithium-ion battery degradation model. *Appl Energy.* 2020;261: 114360.
31. Lai X, Wang SY, Ma SD, Xie JY, Zheng YJ. Parameter sensitiv-ity analysis and simplification of equivalent circuit model for the state of charge of lithium-ion batteries. *Electrochim Acta.* 2019;330:135239.
32. Guo DX, Yang G, Feng XN, Han XB, Lu LG, Ouyang MG. Phys-ics-based fractional-order model with simplified solid phase dif-fusion of lithium-ion battery. *J Energy Storage.* 2020;30:101404.
33. Homan B, ten Kortenaar MV, Hurink JL, Smit GJM. A realistic model for battery state of charge prediction in energy manage-ment simulation tools. *Energy.* 2019;171:205-217.
34. Chen C, Xiong R, Yang RX, Shen WX, Sun FC. State-of-charge estimation of lithium-ion battery using an improved neural network model and extended Kalman filter. *J Clean Prod.* 2019; 234:1153-1164.
35. Couto LD, Schorsch J, Job N, Leonard A, Kinnaert M. State of health estimation for lithium ion batteries based on an equivalent-hydraulic model: an iron phosphate application. *J Energy Storage.* 2019;21:259-271.
36. Zhang C, Allafi W, Dinh Q, Ascencio P, Marco J. Online esti-mation of battery equivalent circuit model parameters and state of charge using decoupled least squares technique. *Energy.* 2018;142:678-688.
37. Farmann A, Sauer DU. Comparative study of reduced order equivalent circuit models for on-board state-of-available-power prediction of lithium-ion batteries in electric vehicles. *Appl Energy.* 2018;225:1102-1122.
38. Wei Z, Hu J, He H, Li Y, Xiong B. Load current and state of charge co-estimation for current sensor-free lithium-ion bat-tery. *IEEE Transactions on Power Electronics.* 2021;99(1):1–12. <http://doi.org/10.1109/tpel.2021.3068725>.
39. Miao H, Chen J, MaoL, QuK, ZhaoJ, Zhu Y. Anovel onlinemodel parameters identification method with anti-interference character-istics for lithium-ion batteries. *International Journal of Energy Research.* 2021;45(6):9502–9517. <http://doi.org/10.1002/er.6477>.
40. Tang XJ, Zhan D, Lyu PX, Rao J, Fan YQ. Online state-of-health estimation of lithium-ion battery based on dynamic parameter identification at multi timescale and support vector regression. *J Power Sources.* 2021;484:229233.

TABLE 1 Mathematical representation of typical electrochemical models

Electrochemical model	Mathematical expression
Shepherd model	$U_L(k) = E_0 - RI(k) - K_1/SOC(k)$
Unnewehr model	$U_L(k) = E_0 - RI(k) - K_2SOC(k)$
Nernst model	$U_L(k) = E_0 - RI(k) - K_3\ln(SOC(k)) + K_4\ln(1 - SOC(k))$

TABLE 2 The equivalent mechanism of each part of the S-ECP model

Mechanism	Mechanism specification
Mechanism 1	The electrodynamic force of this model comes from Nernst empirical equation, whose value is expressed by U_{OC} . The ohm effect of lithium-ion batteries is characterized by internal resistance R_0 in series.
Mechanism 2	The polarization effect of lithium-ion batteries is characterized by the first-order RC parallel circuit.
Mechanism 3	The differences in the charge-discharge internal resistance of lithium-ion batteries are represented by a parallel circuit composed of R_p and C_p .

TABLE 3 Recursive process of F-MILS-based parameter identification

Step 1	Initialize the coefficient matrix and covariance matrix.
Step 2	Obtain the current terminal voltage and operating current measurements.
Step 3	Construct improved multi-innovation matrix and data matrix, as shown in Equation (17). $\mathbf{Y}_{\text{imp}}(n_p, k) = \begin{bmatrix} \left(\gamma + \alpha^{\frac{1}{\tau_p - \tau_p + 1}}\right) [y(k) - \beta^T(k) \hat{\theta}(k-1)] \\ \left(\gamma + \alpha^{\frac{1}{\tau_p - \tau_p + 2}}\right) [y(k-1) - \beta^T(k-1) \hat{\theta}(k-2)] \\ \vdots \\ \left(\gamma + \alpha^{\frac{1}{\tau_p - \tau_p + \tau_p - \tau_p + 1}}\right) [y(k - n_p + 1) - \beta^T(k - n_p + 1) \hat{\theta}(k - n_p)] \end{bmatrix} \quad (17)$
Step 4	Calculate the gain matrix as shown in Equation (18). $K(k) = P(k-1) \beta(n_p, k) [I_{n_p} + \beta^T(n_p, k) P(k-1) \beta(n_p, k)]^{-1} \quad (18)$ where, $P(k-1)$ is the covariance matrix, I_{n_p} is the n_p -order identity matrix.
Step 5	Update the covariance matrix as shown in Equation (19). $P(k) = P(k-1) - K(k) \beta^T(n_p, k) P(k-1) \quad (19)$
Step 6	Update coefficient matrix as shown in Equation (20). $\hat{\theta}(k) = \hat{\theta}(k-1) + K(k) [\mathbf{Y}_{\text{imp}}(n_p, k) - \beta^T(n_p, k) \hat{\theta}(k-1)] \quad (20)$ where, $K(k)$ is the gain matrix.
Step 7	Algorithm iteration cycle until the end.

TABLE 4 Identification results and errors of the improved Nernst model

General model: $U_{OC} = K_0 + K_1 \ln(SOC) + K_2 \ln(1 - SOC)$	Goodness of fit: SSE: 0.002497
Coefficients (with 95% confidence bounds):	R^2 : 0.9912
$K_0 = 3.357 (3.305, 3.408)$	Adjusted R^2 : 0.9883
$K_1 = 0.4218 (0.1918, 0.6517)$	RMSE: 0.0204
$K_2 = -0.1086 (-0.1944, -0.0228)$	

TABLE 5 HPPC test steps

Procedure	Operational Context
Step 1	First, the lithium-ion battery is discharged in a standard discharge. After that, let the battery rest for 2 hours, and then charge the battery to 100% SOC with constant current and voltage. Where, the charging current is set as 1C (50 Ah), the charging voltage is set as 4.2 V, and the cutoff condition is set as 3.4A.
Step 2	Let the battery rest for 12 h to activate the battery and measure and record the voltage values at both ends of the battery.
Step 3	The current pulse test is carried out on the lithium-ion battery. First discharge at 1C current for 10 s, then stand 40 s, and then charge at 1C current for 10 s. The purpose is to make the battery return to the SOC value before discharge and complete a set of pulse charging and discharging tests.
Step 4	Start discharging with 0.5C current, discharge for 12 min (remaining 90% SOC of the battery), and then let it rest for 1 h. The cut-off condition is 3 V.
Step 5	Repeat steps (3) and (4), each cycle discharge 10% capacity, record relevant data, prepare for the next parameter identification.

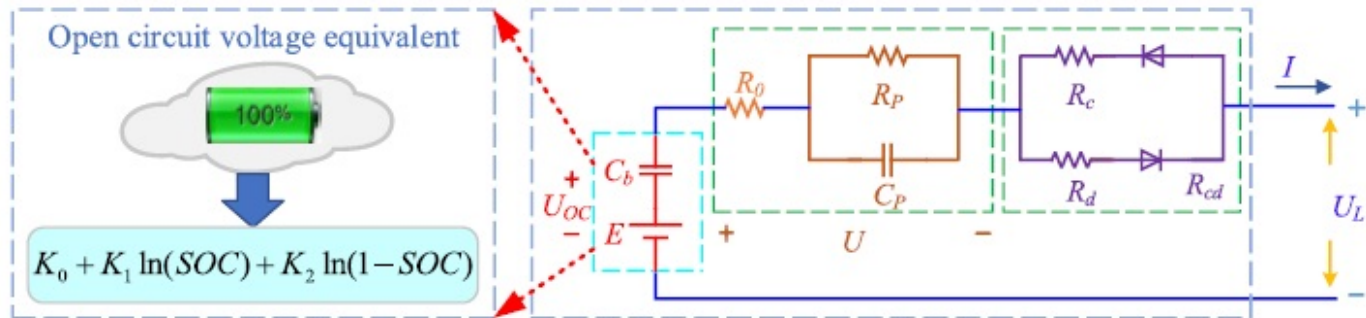
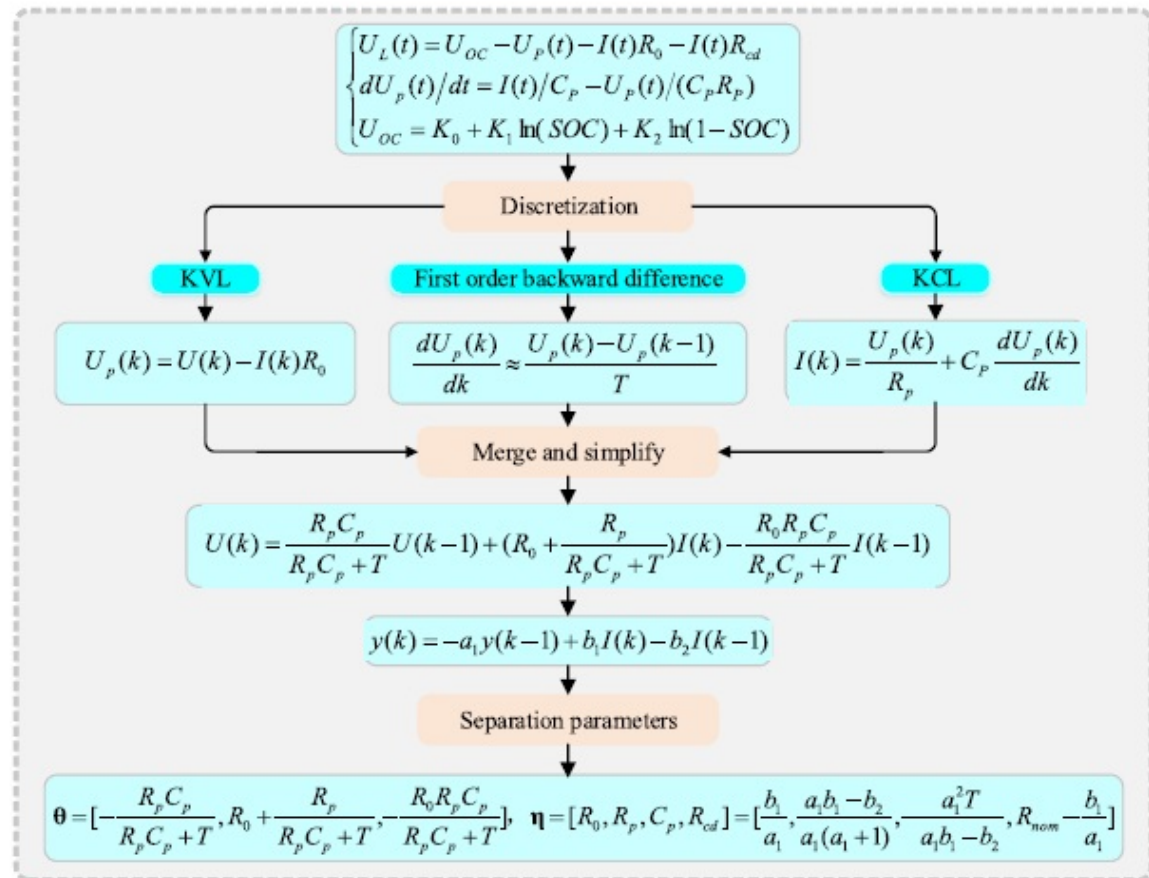


FIGURE 1 S-ECP model for vehicle lithium-ion batteries [Colour figure can be viewed at wileyonlinelibrary.com]

FIGURE 2 Discretization process of the state space equation [Colour figure can be viewed at wileyonlinelibrary.com]



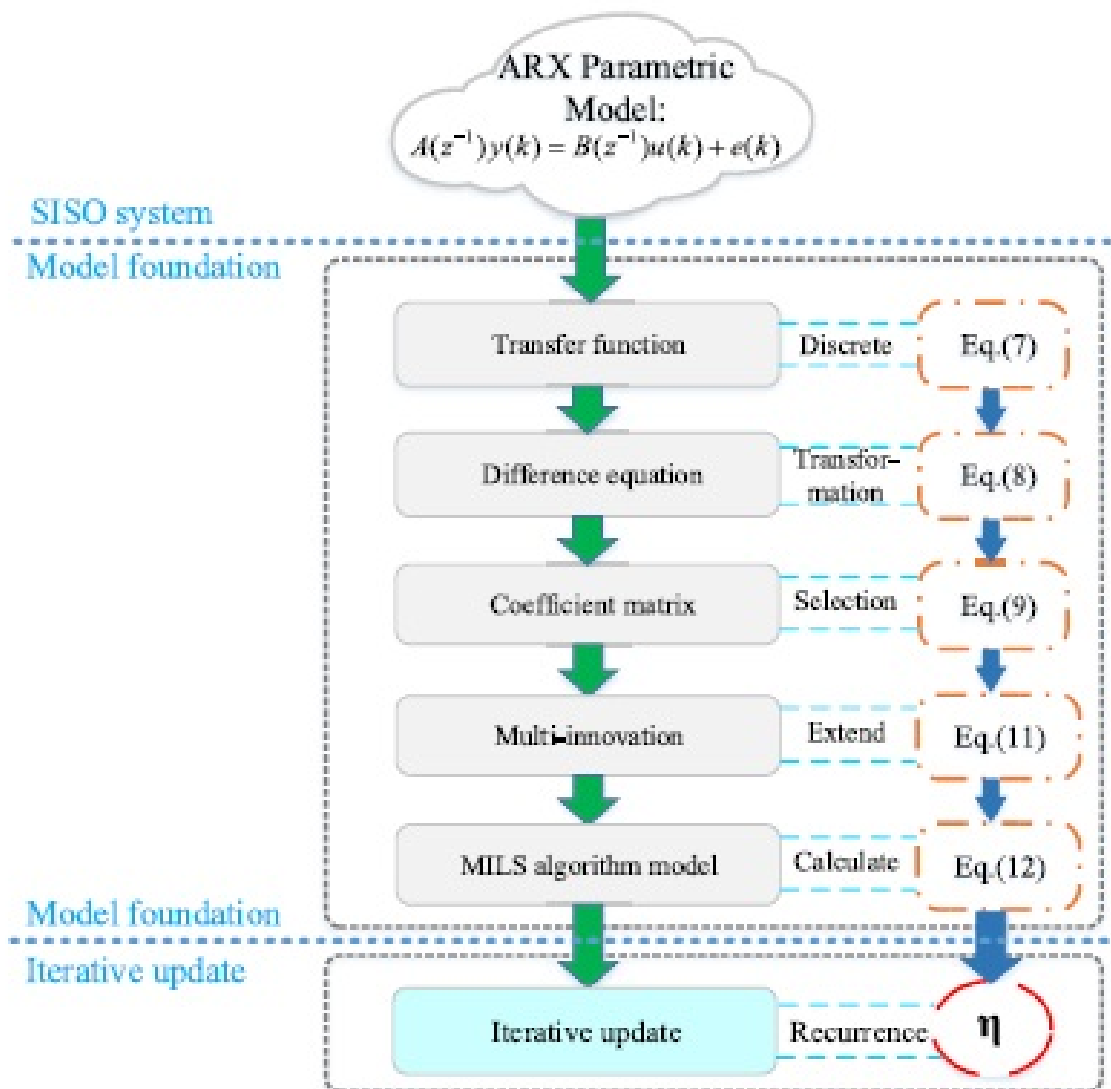


FIGURE 3 MILS model derivation scheme [Colour figure can be viewed at wileyonlinelibrary.com]

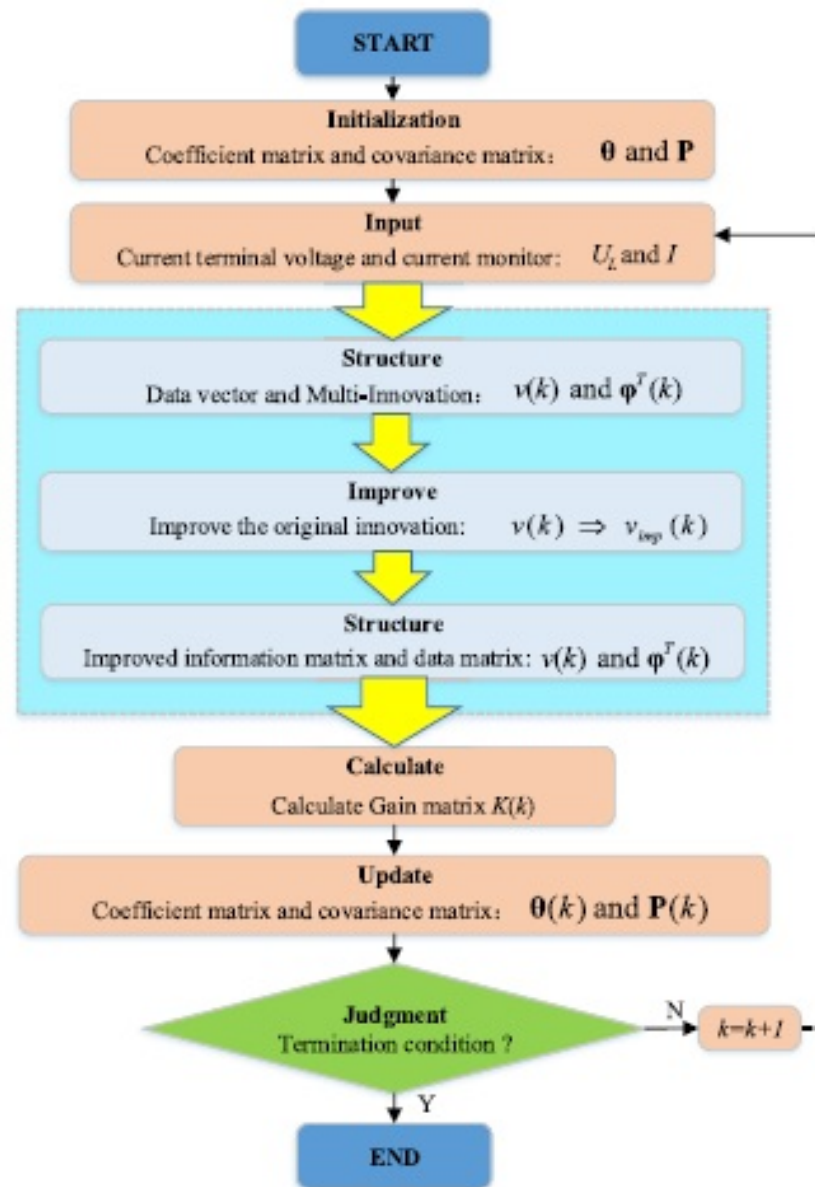


FIGURE 4 F-MILS algorithm flowchart
[Colour figure can be viewed at
wileyonlinelibrary.com]

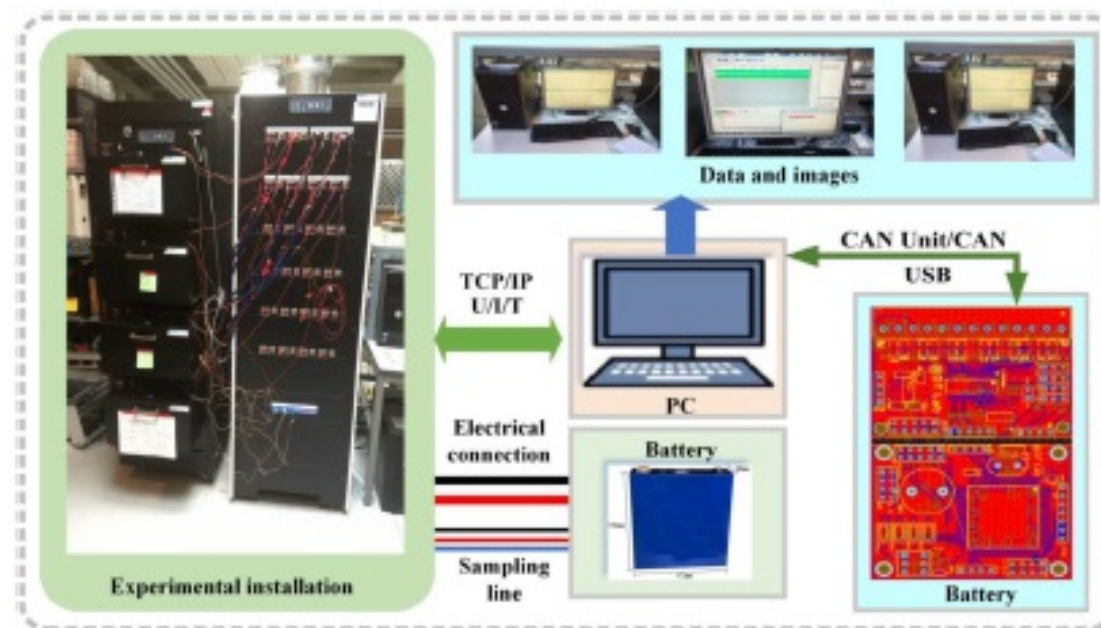


FIGURE 5 Experimental lithium-ion battery test platform [Colour figure can be viewed at wileyonlinelibrary.com]

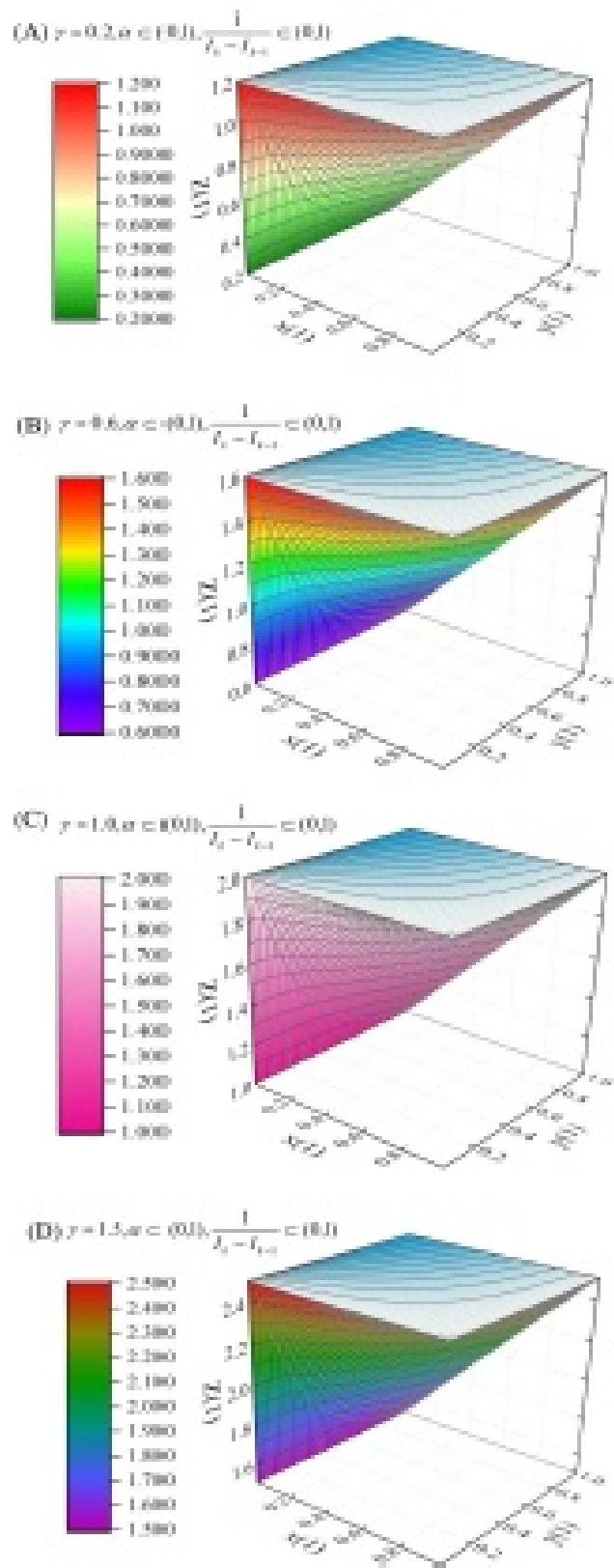


FIGURE 6 Results of the search in region of weight constraint factors [Colour figure can be viewed at [wileyonlinelibrary.com](http://www.wileyonlinelibrary.com)]

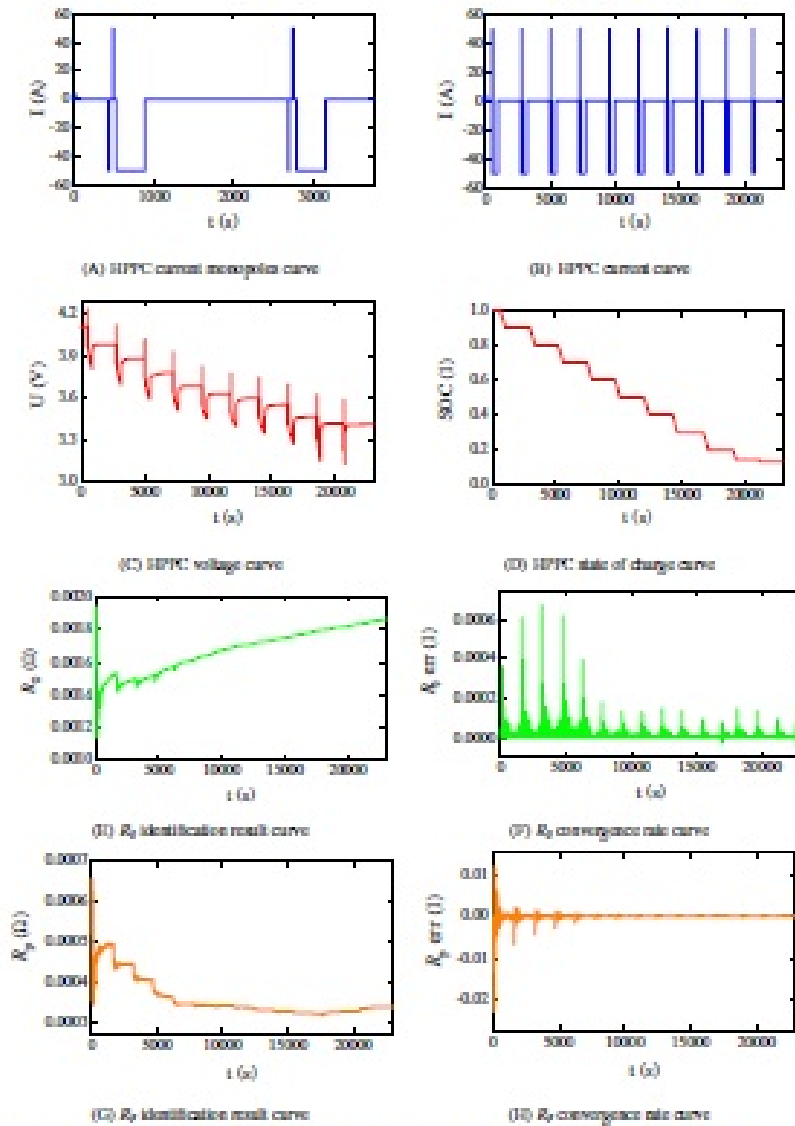


FIGURE 7 HPPC test and parameter identification results [Colour figure can be viewed at wileyonlinelibrary.com]

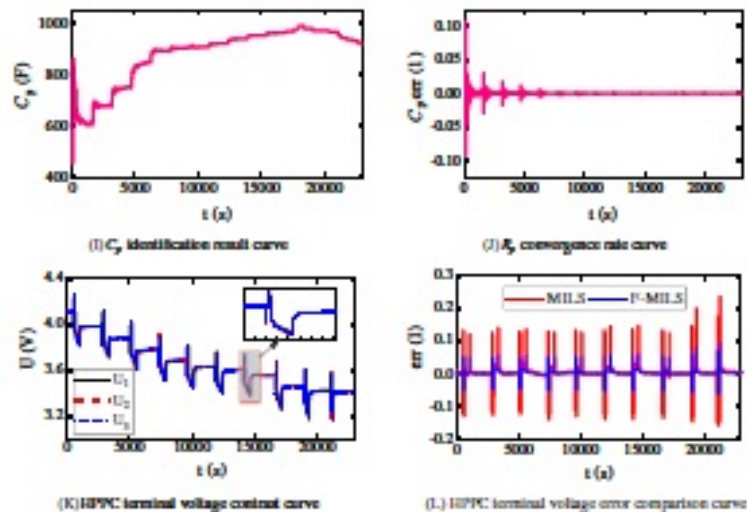


FIGURE 7 (Continued)

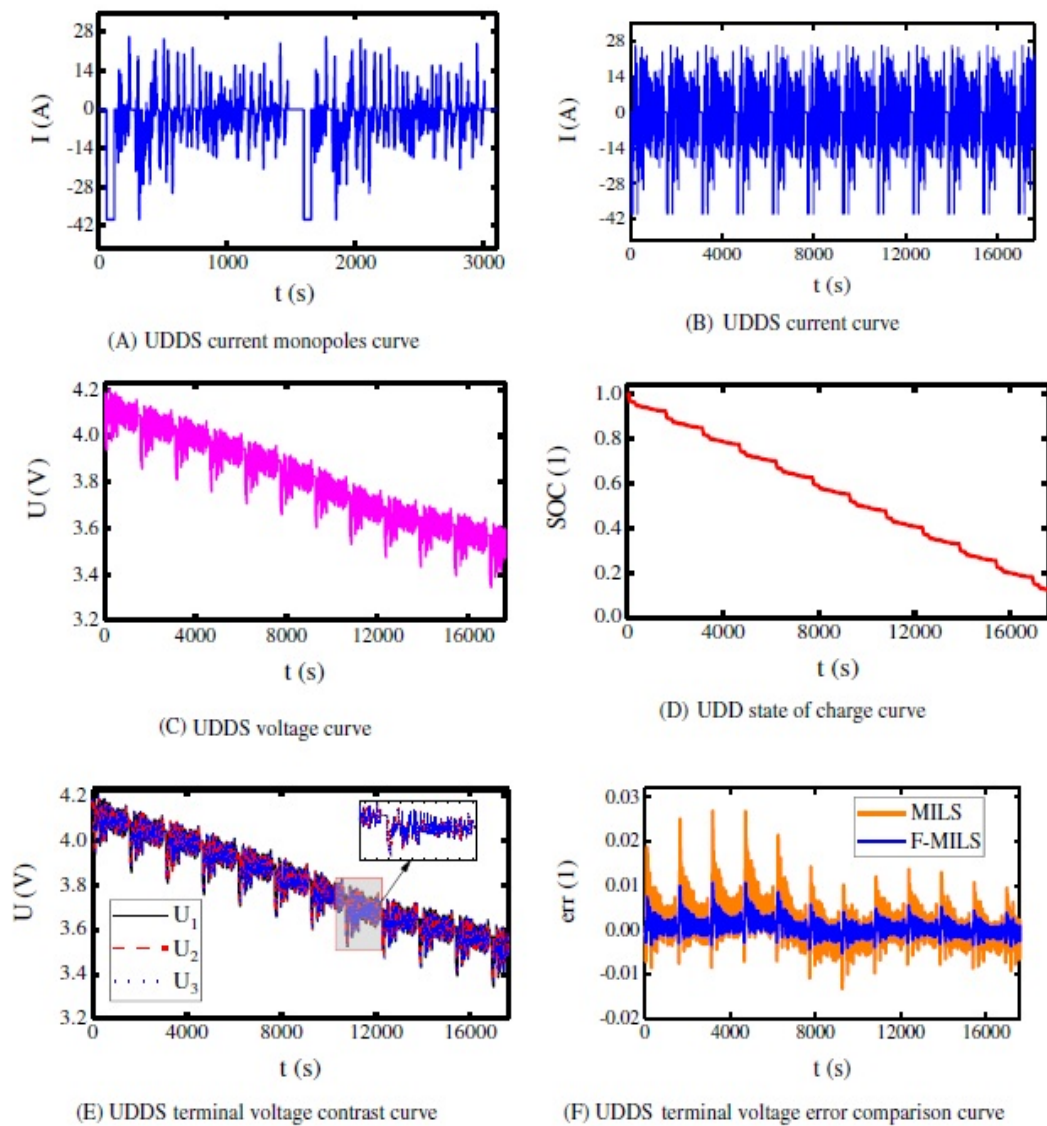


FIGURE 8 UDDS test and error comparison [Colour figure can be viewed at wileyonlinelibrary.com]